ISSN 0021-3640, JETP Letters, 2024, Vol. 119, No. 11, pp. 813–822. © The Author(s), 2024. This article is an open access publication.
Russian Text © The Author(s), 2024, published in Pis'ma v Zhurnal Eksperimental'noi i Teoreticheskoi Fiziki, 2024, Vol. 119, No. 11, pp. 785–795.

FIELDS, PARTICLES, AND NUCLEI

Test of the Model of "Running Axial Mass" Using NOvA Near Detector Data on Muon Neutrino Scattering on Nuclei

I. D. Kakorin[a,*], V. A. Naumov[a,], and O. B. Samoylov[a,b,***]**

[a] *Joint Institute for Nuclear Research, Dubna, Moscow region, 141980 Russia*
[b] *Institute for Nuclear Research, Russian Academy of Sciences, Moscow, 117312 Russia*
**e-mail: kakorin@jinr.ru*
***e-mail: vnaumov@theor.jinr.ru*
****e-mail: samoylov@jinr.ru*

Received April 17, 2024; revised April 23, 2024; accepted April 25, 2024

A phenomenological model of a "running axial mass" (MArun) was previously proposed to calculate cross sections for the quasielastic scattering of neutrinos and antineutrinos on nuclei. It can be easily implemented in neutrino generators and has only two free parameters, which are obtained from the global fit to the experimental data on the total and differential cross sections for the quasielastic scattering of (anti)neutrinos on various nuclear targets. In this work, the NOvA near detector data on the total and differential cross sections for the scattering of muon neutrinos, are compared to the simulation performed using the GENIE neutrino Monte Carlo generator (v.3.4.0), which optionally allows for using the MArun model.

DOI: 10.1134/S0021364024601271

1. INTRODUCTION

The detailed experimental and theoretical study of cross sections for the interactions of neutrinos with nuclei in a wide kinematic region is necessary for verifying the Standard Model and phenomenology inspired by it, for numerous astrophysical applications, and for processing and interpretation of experiments on studying the neutrino properties beyond the Standard Model, in particular, neutrino oscillation experiments.

In modern long-baseline accelerator experiments with two (near and far) detectors (e.g., NOvA [1] and T2K [2]), it is customary to fine-tune the interaction model to the near detector measurement data. This fine tuning is certainly necessary but does not completely eliminate uncertainties of the model in its extrapolation to the far detector, which receives a neutrino energy spectrum distorted compared to the spectrum in the near detector even if the detectors are arranged coaxially because neutrinos only from a small solid angle near the beam axis reach the far detector.

Individual tunings of interaction models are obviously inapplicable for the joint analysis of several experiments. At the same time, the planned next-generation experiments such as DUNE [3], T2HK [4], T2HKK [5], and P2O [6] will require a qualitative, several-fold increase in the accuracy of the cross section calculations, which cannot be achieved in the current state of theory. For this reason, the joint analysis of neutrino oscillation experiments should seemingly involve universal (microscopic and phenomenological) models tested or fitted on the possible widest set of data of independent accelerator experiments with different targets in a wide energy range.

In this work, one of such phenomenological models [7–9], which is developed to describe the quasielastic scattering of neutrinos and antineutrinos on nuclei and is implemented in the GENIE neutrino Monte Carlo generator [10], is compared to recently reported results of measurements of the charged-current interactions of muon neutrinos in the NOvA near detector [1].

The NOvA data are presented as the neutrino-spectrum-averaged inclusive cross sections: double differential, $d^2\sigma/d\cos\theta_\mu dT_\mu$, and differential, $d\sigma/dQ^2$, as well as the ratio of the total cross section $\sigma(E_\nu)$ to the neutrino energy E_ν, where T_μ is the kinetic energy of the muon, θ_μ is the muon emission angle with respect to the momentum of the neutrino, and Q^2 is the absolute value of the square of the 4-momentum transfer from the neutrino to the muon.

The elemental composition of the detector and the energy spectrum of the ν_μ beam should be carefully taken into account to calculate cross sections. Since this spectrum is fairly wide, events in the detector are

generated from interactions of many types from quasielastic to deep inelastic. All of them, as well as secondary interactions with the nucleus of hadrons produced in inelastic collisions, are simulated using the GENIE neutrino Monte Carlo generator (v.3.4.0) without any tuning to NOvA near detector data. The results are also compared to predictions of several other popular models.

2. CHARACTERISTICS OF THE DETECTOR AND THE NOvA BEAM

The near detector (ND) is a $4 \times 4 \times 16$-m track calorimeter with an active mass of 193 ton, which consists of vertical and horizontal rectangular polyvinylchloride cells 3.9 cm in width, 3.9 m in length, and depth 6.6 cm in the beam direction, filled with a liquid scintillator consisting of 95% mineral oil and 5% 1, 2, 4-trimethylbenzene with small concentrations of wavelength-shifting fluors. The resulting working volume of the near detector contains 67 wt % of carbon, 16 wt % of chlorine, 11 wt % of hydrogen, 3 wt % of titanium, 3 wt % of oxygen, and <1 wt % of other elements.

The NuMI (Neutrinos at Main Injector) accelerator complex at the Fermi National Laboratory (United States) in the so-called "neutrino configuration" provides the ν_μ beam with an admixture of 1.8% of $\overline{\nu}_\mu$ and 0.7% of $\nu_e + \overline{\nu}_e$ at $E_\nu = 1$–5 GeV. Neutrinos and antineutrinos are produced in decays of pions, kaons, and secondary muons in a 650-m decay channel. Pions and kaons are produced in the collisions of 120-GeV protons from the Main Injector (proton synchrotron) with a graphite target and are focused by a pair of magnetic horns. The near detector is located at an angle of 14.6 mrad to the central axis of the neutrino beam. The ν_μ spectrum has a characteristic narrow pion peak at an energy of $E_\nu \simeq 1.8$ GeV and a wide kaon peak at $E_\nu \simeq 12$ GeV. The intensity of ν_μ at $E_\nu = 20$ GeV is almost 420 times smaller than the maximum value.

3. SIMULATION

In the GENIE neutrino Monte Carlo generator (v.3.4.0), collisions of (anti)neutrinos with nuclei are simulated independently for each of the quasielastic, resonant, deep-inelastic, etc. channels using specialized models and taking into account their relative contributions to the total number of events. Several interchangeable models are usually used in the generator for each type of processes to construct the so-called comprehensive model configurations (CMCs).

To simulate quasielastic events, we used the Smith–Moniz relativistic Fermi gas model [11] (with a small modification [12] and refined Fermi momenta and binding energies, which are the parameters of the relativistic Fermi gas) with the MArunAxialFormFactorModel option involving the empirical model with running axial mass (MArun). This model was proposed to calculate cross sections for quasielastic [7, 8] and quasielastic-like charged-current interactions [9] of neutrinos and antineutrinos with nuclei. For this, instead of the constant axial mass of the nucleon M_A in the standard dipole parameterization of the axial form factor $F_\mathrm{A}(Q^2) = F_\mathrm{A}(0)/(1 + Q^2/M_\mathrm{A}^2)^2$, it was proposed to use the running axial mass depending on the neutrino energy, which can be parameterized in the laboratory reference frame by the simple formula $M_\mathrm{A}^\mathrm{run} = M_0(1 + E_0/E_\nu)$. Here, $E_\nu = (s - M^2)/2M$, where M is the mass of the nucleon and s is the Mandelstam variable, is the energy treated as a Lorentz invariant and M_0 and E_0 universal (independent of the target nucleus) constants determined from the global fit to the existing (in 2013) accelerator experiment data on cross sections for the quasielastic and quasielastic-like scatterings of (anti)neutrinos on nuclei, including precise results of the NOMAD experiment [13] (total cross sections) and the MiniBooNE experiment [14, 15] (double differential cross sections).

The parameters M_0 and E_0 found in [8, 9] are $M_0 = (1.008 \pm 0.025)$ GeV and $E_0 = 331^{+57}_{-54}$ MeV. The constant M_0 can be interpreted as the current axial mass because effects of the relativistic Fermi gas at high energies $E_\nu \gg E_0$ can be neglected with a high accuracy and scattering can be treated as occurring on a free nucleon. The M_0 value indeed agrees within the errors with the value $M_A^\mathrm{D} = 1.003 \pm 0.083$ GeV, which was extracted from the data obtained on deuterium targets with allowance for effects of meson exchange currents in the one-pion exchange approximation in the static limit. It also agrees with the results of previous global analyses [7, 12]. In addition, the MArun model satisfactorily describes numerous data of the T2K ND280 [16, 17], MINERvA [18, 19], and MiniBooNE [14, 15, 20] experiments that were not involved in the fit and where effects of meson exchange currents are empirically taken into account through the energy dependence of M_A^run. The model obviously cannot describe in detail data in the kinematic regions, where the contribution of meson exchange currents dominates (e.g., data on the exclusive and semi-inclusive reactions with the detection of a pair of the final nucleons).

To calculate the neutrino-induced production of pions, we used the "extended" Rein–Sehgal model [21], which was adapted to the features of the GENIE generator and is known as the KLN–BS model abbreviated after its authors [22, 23]. The polarization and mass of the final charged lepton [22], as well as the contribution of the pion pole to the hadron axial current [23], were included in this model. For some reasons, the current version of the GENIE generator, as well as its earlier versions, involve not all aspects of the

KLN–BS model. The most important modifications (often these are forced simplifications) are listed below.

• Interference between resonances with identical spins and orbital angular momenta of the final $N\pi$ state is disregarded in order to simplify including the multiple production of pions and other light mesons in the simulation. These processes should be taken into account to correctly describe neutrino interactions in the kinematic region intermediate between the resonant and deep inelastic regions.

• Instead of the nonresonant mechanism of pion production used in the Rein–Sehgal and KLN–BS models, the GENIE generator involves a more universal semiempirical sewing mechanism in the mentioned intermediate kinematic region.

• To avoid the double count, nonphysical tails of resonances are cut in the region of their overlapping.

In this calculations, we made two additional significant changes.

• The renormalization introduced in [21] for the Breit–Wigner functions approximating the shape of the resonances was not used for the reasons presented in detail in [24].

• For the important parameter of the model known as the "resonance" axial mass M_A^{RES}, we used a value of (1.18 ± 0.07) GeV obtained from the global fit to the data on the neutrino-induced single-pion production in the ANL, BNL, FNAL, and CERN experiments with deuterium and hydrogen bubble chambers [24]. The main reasons for the difference of the new M_A^{RES} value from a default value of (1.12 ± 0.06) GeV, which was obtained in the preceding global analysis [25] (including also data on nuclei heavier than deuteron) and is used in the GENIE generator and in some other neutrino generators, are the improvement of the fitting procedure, the inclusion of current data on the parameters of nucleon and baryon resonances (masses and total and partial widths) [26], the correction of some ANL and BNL data [27], and the joint fitting of M_A^{RES} and the parameter f_{NRB} specifying the general scale for the nonresonant neutrino-induced single-pion production.

To simulate events from other contributions (deep inelastic, coherent, diffraction, etc.), we used the same models as for the GENIE CMC G18_10a [10].

4. COMPARISON OF THE EXPERIMENTAL DATA WITH THE MONTE CARLO SIMULATION

In the calculations, we used the elemental composition of the target in the NOvA near detector discussed above and the energy spectrum of ν_μ with the energies $E_\nu < 20$ GeV from [1], but with a more detailed binning. The double and single differential cross sections presented below should be considered as inclusive cross sections averaged over the energy spectrum. Figure 1 presents the measured double differential inclusive cross sections $d^2\sigma/d\cos\theta_\mu dT_\mu$, in comparison with the Monte Carlo simulation in the model with running axial mass.

Figure 2 shows similar data for the differential cross section $d\sigma/dQ^2$ and the total cross section $\sigma(E_\nu)$ divided by the neutrino energy E_ν. Histograms with different shades present contributions from three main processes—quasielastic (including quasielastic-like), resonant single-pion production and deep inelastic—to the inclusive cross section. The summary cross section includes all these contributions and all other relatively small contributions such as multiple production of light mesons, coherent and diffraction interaction, and charm production. The latter contributions are most noticeable at small angles when $\cos\theta_\mu \gtrsim 0.98$. For all types of interactions, we took into account intranuclear cascade and finite-state interaction effects included in the GENIE generator (v.3.4.0).

The simulation well describes the data presented in Fig. 1 at $0.50 < \cos\theta_\mu < 0.91$. The model systematically underestimates the data outside of this region: at comparatively high kinetic energies of the muon (i.e., to the right of the peaks) for bins with $0.91 < \cos\theta_\mu < 0.99$ and at low energies (i.e., to the left of the peaks) for bins with $0.99 < \cos\theta_\mu < 1$. The resulting distribution obtained by joining all angular ranges with $\cos\theta_\mu > 0.5$ (see the lower right panel of Fig. 1) underestimates the experimental data for about one third of all bins but by no more than one standard deviation.

The calculation of the differential cross section $d\sigma/dQ^2$ (see Fig. 2a) is in good agreement with the data at all values of the four-momentum transfer squared except for only the penultimate bin. The calculated ratio $\sigma(E_\nu)/E_\nu$ is in agreement with experimental data in the entire energy range $0.5\ \mathrm{GeV} < E_\mu < 5$ GeV except for three bins, where discrepancies exist but are small.

For more objective quantitative comparison, we discuss here the results of a more detailed analysis including correlations of data uncertainties and with the comparison of the calculations performed in [1] for some competitive models of the interaction of neutrinos with nuclei. In addition to the basic GENIE v2.12.2–NOvA Tune model [28], which is based on the GENIE generator (version 2.12.2) [29, 30] but is significantly upgraded and tuned for the best agreement with the NOvA near detector data [1], we considered the original (not adapted to the NOvA data) model, which is incorporated in the GENIE generator (v2.12.2), and the model (CMC) N18-10j-02-11a, which enters the later 3.00.06 version of the GENIE generator [31, 32]. Furthermore, we discuss the mod-

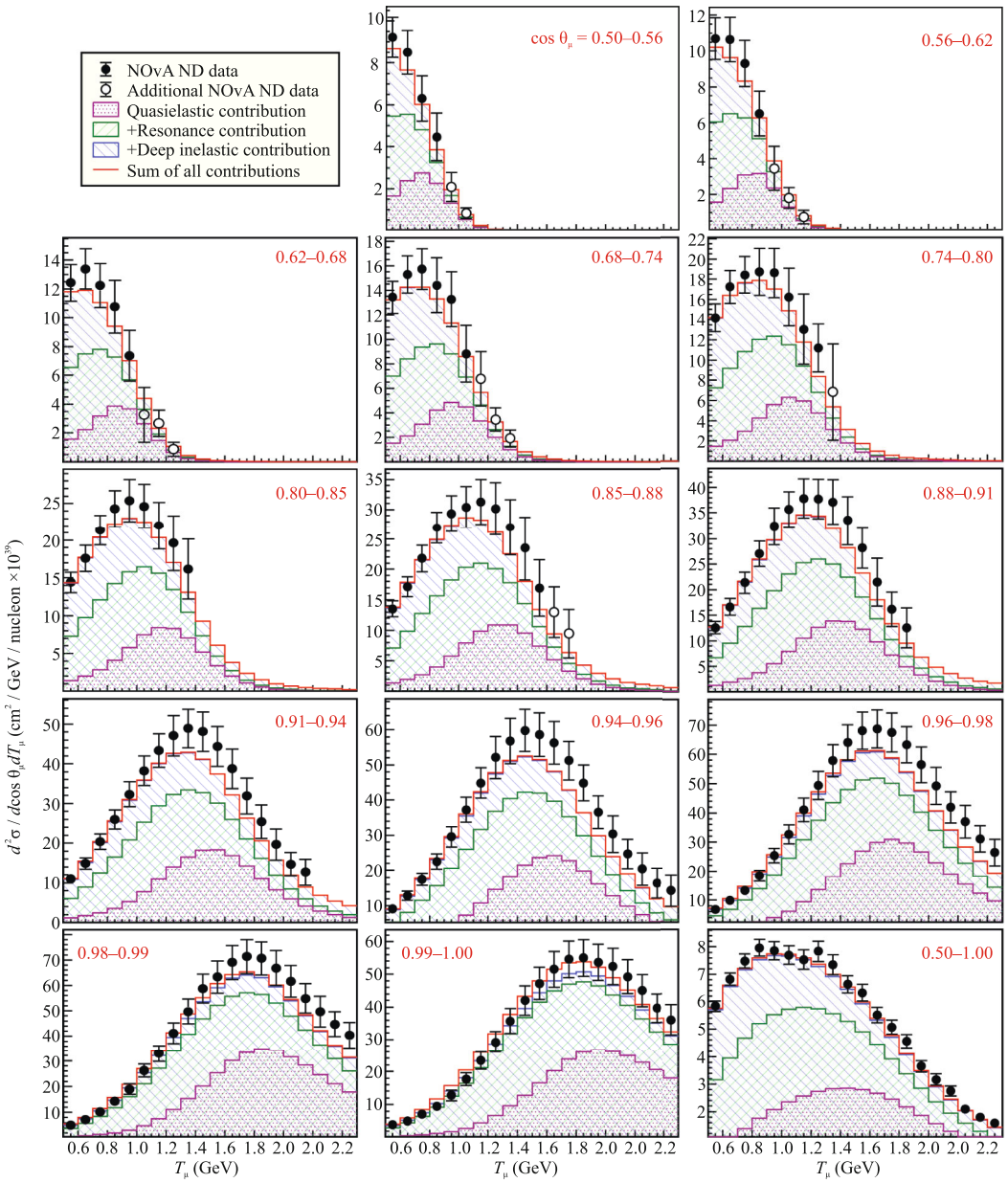

Fig. 1. (Color online) Double differential inclusive cross section $d^2\sigma/d\cos\theta_\mu dT_\mu$ for the charged-current scattering of ν_μ on nuclei measured in the NOvA near detector [1] for $\cos\theta_\mu$ ranges indicated in the corresponding panels in comparison with the simulation using the GENIE neutrino Monte Carlo generator (v.3.4.0) with the running axial mass (MArun) option; details of the simulation are described in the main text. The quasielastic, resonance, and deep inelastic contributions to the total cross section are presented by histograms with different shades (see the legend). The filled and empty circles with total error bars are the experimental data involved in the final NOvA analysis and additional data, respectively. The bottom right panel shows the cross section obtained by joining all $\cos\theta_\mu$ ranges.

els included in NEUT v5.4.0 [33–35] and NuWro [36, 37] Monte Carlo neutrino generators, as well as in the GiBUU [38, 39], which is a more general tool to simulate hadronic and electroweak reactions on nuclei. All these generators are widely used to design experiments with accelerator and atmospheric neutrinos and to process and interpret their results. Their main features and comparative characteristics can be found in reviews [40, 41].

To compare the calculations and data, we used the three quantities

$$\chi^2_{\text{diag}} = \sum_i \frac{(E_i - T_i)^2}{\sigma_i^2}, \quad (1)$$

$$\chi^2_{\text{tot}} = (\mathbf{E} - \mathbf{T})^T \mathbf{W}^{-1}_{\text{tot}} (\mathbf{E} - \mathbf{T}), \quad (2)$$

$$\chi^2_{\text{sh}} = (\mathbf{E} - N\mathbf{T})^T \mathbf{W}^{-1}_{\text{sh}} (\mathbf{E} - N\mathbf{T}) + \frac{(N-1)^2}{\delta^2}. \quad (3)$$

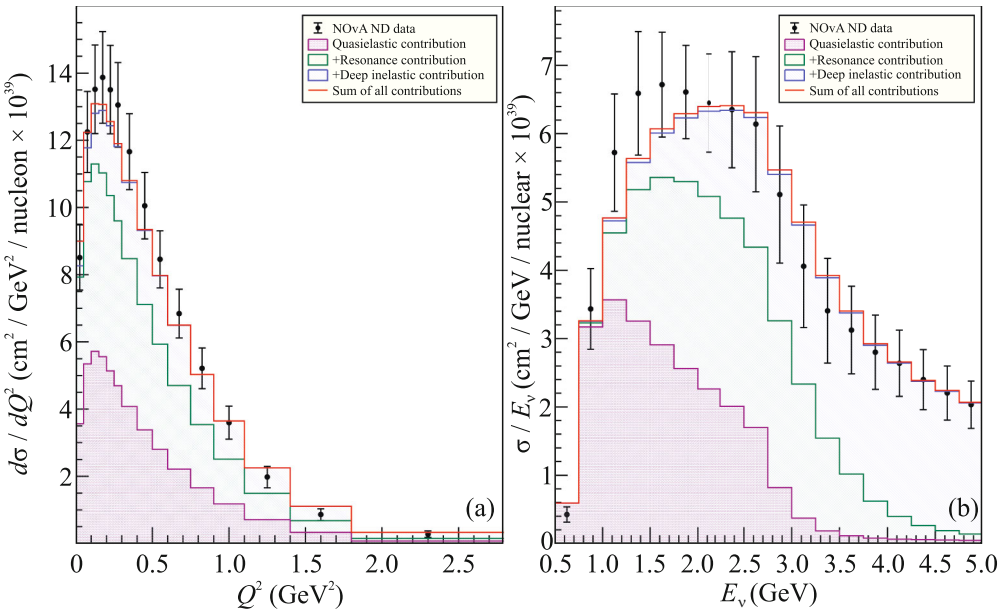

Fig. 2. (Color online) (a) Differential inclusive cross section $d\sigma/dQ^2$ for the charged-current scattering of ν_μ on nuclei and (b) the total cross section $\sigma(E_\nu)$ divided by the neutrino energy E_ν measured in the NOvA near detector [1] in comparison with the simulation using the GENIE neutrino Monte Carlo generator (v.3.4.0) with the MArun option; details of the simulation are described in the main text. The notation is the same as in Fig. 1.

Here, **E** and **T** are the vectors composed from bin-averaged experimental data E_i and model predictions T_i, respectively; $\mathbf{W}_{\text{tot}} = \|W_{ij}\|$ is the total covariance matrix; $\mathbf{W}_{\text{sh}}$ is the shape covariance matrix, which corresponds to the dependence of the data on the measured kinematic variables and disregard uncertainties in the general normalization of the data; $\delta = 11.2\%$ is the average relative uncertainty of the general normalization; and $\sigma_i = \sqrt{W_{ii}}$ is the total measurement uncertainty for the ith bin. All data are taken from the free-access NOvA Collaboration site [42].

The correlation matrices corresponding to the covariance matrices $\mathbf{W}_{\text{tot}}$ and $\mathbf{W}_{\text{sh}}$ for three types of data are shown in Figs. 3–5. In particular, it is seen in these figures that most data of each type are strongly correlated (see panels (a) in Figs. 3–5), but regions with weak correlation and even with strong anticorrelation (see panels (b) in Figs. 3–5) appear after the subtraction of covariances caused by uncertainties of normalizations of the flux and cross sections from the total covariance matrix $\mathbf{W}_{\text{tot}}$. The correlation coefficients and covariances vary significantly in different regions of the kinematic variables T_μ, θ_μ, Q^2, and E_ν.

A nontrivial structure of correlation matrices shows that the estimate of the quality of data description by means of χ^2_{diag} would be not only too rough but would often provide opposite conclusions. For this reason, we below present such estimates only to illustrate that it is important to take into account correlations. We also note that the comparison of the χ^2_{tot} and χ^2_{sh} values presented below is senseless because the covariance matrix $\mathbf{W}_{\text{sh}}$ does not include dominant contributions to systematic errors and covariances and χ^2_{sh} contains a penalty term. Only χ^2 characteristics of the same type calculated for different interaction models should be compared to each other.

The estimate $\delta = 11.2\%$ given above was obtained as a weighted average value over uncertainties of all bins of the measured double differential cross section. The dominant contribution to δ comes from the uncertainty of the neutrino flux, which reaches $\pm 20\%$ and $\pm 15\%$ at $E_\nu \lesssim 200$ MeV and $E_\nu \gtrsim 4$ GeV, respectively, and is $\pm 9.1\%$ on average. The contributions from all normalization uncertainty sources are almost fully correlated with each other and with other systematic errors. Statistical errors, which are $\pm 1.6\%$ on average, correlate very weakly with the systematic errors: the weighted average correlation coefficient is 0.0031 (cf. 0.71 for the averaged total systematic error).

The normalization coefficient N in Eq. (3) is determined from the minimum condition $\partial\chi^2_{\text{sh}}/\partial N = 0$ as

$$N = \frac{1 + \delta^2 \mathbf{T}^T \mathbf{W}_{\text{sh}}^{-1} \mathbf{E}}{1 + \delta^2 \mathbf{T}^T \mathbf{W}_{\text{sh}}^{-1} \mathbf{T}}. \quad (4)$$

Obviously, $N \to 1$ as $\delta \to 0$. The dependence of N on δ is weakened with increasing δ. The dependence of N on δ for the NOvA data becomes insignificant at $\delta \gtrsim 9\%$. In view of this circumstance, we also used the

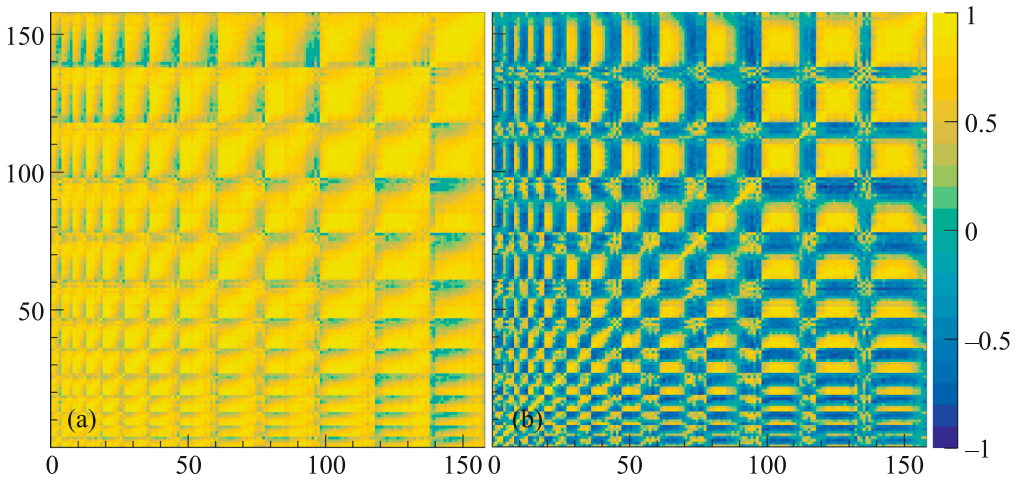

Fig. 3. (Color online) Correlation matrices corresponding to the covariant matrices (a) $\mathbf{W}_{tot}$ and (b) $\mathbf{W}_{sh}$ for $d^2\sigma/d\cos\theta_\mu dT_\mu$. The bins are enumerated from left to right and from top to bottom according to the first 13 panels of Fig. 1. The color scale on the right refers to the both panels.

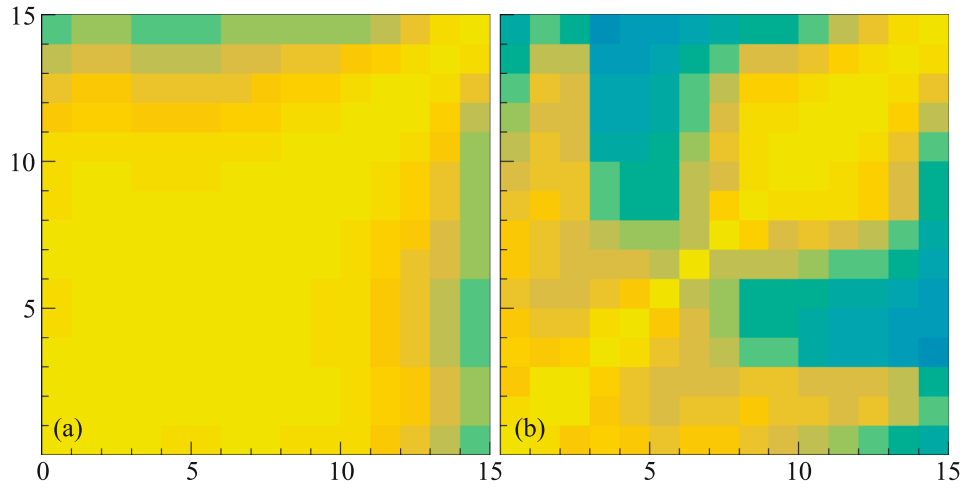

Fig. 4. (Color online) Correlation matrices corresponding to the covariant matrices (a) $\mathbf{W}_{tot}$ and (b) $\mathbf{W}_{sh}$ for $d\sigma/dQ^2$. The bins are enumerated in the direction of increasing Q^2 in Fig. 2a. The color scale is the same as in Fig. 3.

estimate $\delta = 11.2\%$ to analyze the data on $d\sigma/dQ^2$ and $\sigma(E_\nu)/E_\nu$.

The normalization coefficients with the total uncertainty for three types of data and seven models, which were evaluated with the standard normalization of the calculations to the area used in [1], are summarized in Table 1, where the normalization uncertainty estimated from the diagonal terms of the matrix $\mathbf{W}_{tot}$, i.e., disregarding correlations are also presented for comparison. It is seen that the ignorance of correlations underestimates the real uncertainty by a factor of 8.2 (!) for $d^2\sigma/d\cos\theta_\mu dT_\mu$ and by a factor of 3.3 for $d\sigma/dQ^2$ and $\sigma(E_\nu)/E_\nu$. Even this simple example well illustrates the decisive role of correlations in the quantitative comparison of model calculations with NOvA data.

The normalization coefficients N obtained by normalizing to the area are not optimal because they do not ensure the best description of the data in shape. Consequently, they can (and generally should) differ from the corresponding normalization coefficients N calculated by Eq. (4). These differences are clearly seen when comparing the normalizations presented in Tables 1 and 2: the difference in some cases is no more than 0.5% but more often reaches several percent up to 8.8%. This difference is always with margin within the total errors presented in Table 1; i.e., two normalization methods formally are not contradictory.

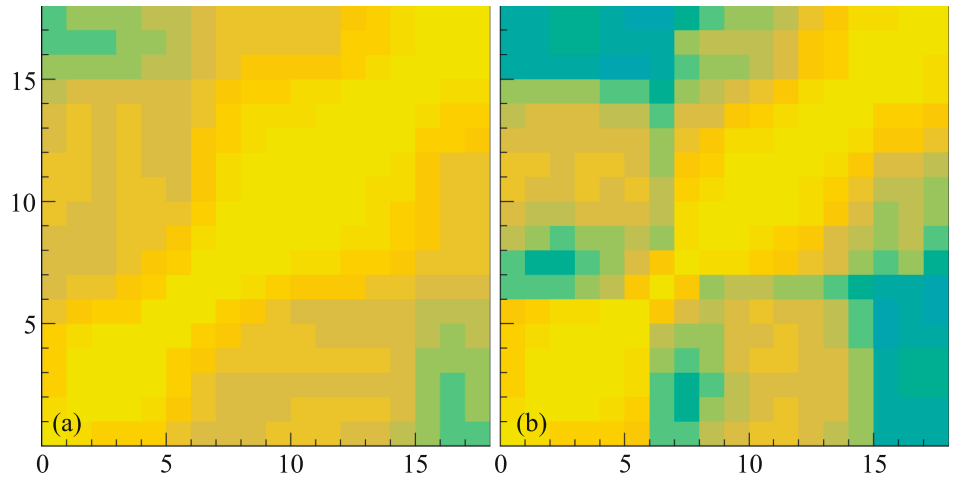

Fig. 5. (Color online) Correlation matrices corresponding to the covariant matrices (a) $\mathbf{W}_{tot}$ and (b) $\mathbf{W}_{sh}$ for $\sigma(E_\nu)/E_\nu$. The bins are enumerated in the direction of increasing E_ν in Fig. 2b. The color scale is the same as in Fig. 3.

The ratios of the cross sections $d^2\sigma/d\cos\theta_\mu dT_\mu$ calculated in several models of the neutrino–nucleus interactions and averaged over the spectrum of neutrinos to the corresponding experimental data are presented in Fig. 6 in the linear binning representation, as described in detail in the caption. Figures 6a and 6b show these ratios for absolute (unrenormalized) model predictions and for renormalized predictions with the normalization coefficients given by Eq. (4) derived by minimizing the function χ^2_{sh}. The found normalization coefficients and three χ^2 characteristics are summarized in Table 2.

The data shown in Figs. 1 and 6 by empty circles (14 bins) have comparatively large statistical and systematic errors and are excluded from the official analysis of the NOvA data. They are not involved in the calculation of the normalization factors and χ^2 values presented in Table 2 and are shown here to demonstrate that the MArun model does not contradict these data.

As seen in Fig. 6 and Table 2, unrenormalized predictions by different models are inconsistent with each other. Discrepancies between models decrease significantly after renormalizations, but the normalization coefficients required for the best agreement with data vary in the wide range from 0.98 (GENIE 2.12.2) to 1.29 (GiBBU 2019), i.e., within about 2.7δ. No one of the presented models obviously cannot compete with the NOvA Tune model whose free parameters are specially tuned to the NOvA near detector data on $d^2\sigma/d\cos\theta dT_\mu$ and which thereby does not require additional renormalization. Nevertheless, the NuWro 2019 and MArun models give close χ^2_{diag}, χ^2_{tot}, and χ^2_{sh} values smallest except for the NOvA Tune model. The MArun model requires a significant renormalization with the coefficient $N \simeq 1.11 \simeq 1 + 0.94\delta$ (cf.

Table 1. Normalization coefficients (with total uncertainties), which are required for the standard normalization of the quantities $d^2\sigma/d\cos\theta_\mu dT_\mu$, $d\sigma/dQ^2$, and $\sigma(E_\nu)/E_\nu$ to the area, as calculated in seven models of the interaction of neutrinos with nuclei. The relative normalization uncertainties estimated for these quantities using the total covariance matrices $\mathbf{W}_{tot}$ are 9.76, 9.73, and 12.5%, respectively. The total absolute uncertainties obtained disregarding correlations are given in square brackets for comparison. The corresponding relative errors are 1.19, 2.94, and 3.79%, respectively

Model	$d^2\sigma/d\cos\theta_\mu dT_\mu$ (158 bins)	$d\sigma/dQ^2$ (15 bins)	$\sigma(E_\nu)/E_\nu$ (18 bins)
GENIE 2.12.2	0.974 ± 0.095[0.012]	0.942 ± 0.092[0.028]	0.943 ± 0.117[0.036]
GENIE 3.00.06	1.088 ± 0.106[0.013]	1.126 ± 0.109[0.033]	1.086 ± 0.135[0.033]
NEUT 5.4.0	0.996 ± 0.097[0.012]	0.987 ± 0.096[0.029]	1.015 ± 0.126[0.039]
GiBBU 2019	1.329 ± 0.130[0.016]	1.279 ± 0.124[0.038]	1.275 ± 0.159[0.048]
NuWro 2019	1.145 ± 0.112[0.014]	1.139 ± 0.111[0.033]	1.143 ± 0.142[0.043]
NOvA Tune	1.008 ± 0.098[0.012]	0.977 ± 0.095[0.029]	0.960 ± 0.120[0.036]
MArun	1.069 ± 0.104[0.013]	1.018 ± 0.099[0.030]	1.011 ± 0.126[0.038]

Table 2. Parameters χ^2_{diag}, χ^2_{tot}, and χ^2_{sh} calculated for $d^2\sigma/d\cos\theta_\mu dT_\mu$, $d\sigma/dQ^2$, and $\sigma(E_\nu)/E_\nu$ and the normalization coefficients N determined from the minimization of χ^2_{sh} for seven models of the interaction of neutrinos with nuclei

Model	$d^2\sigma/d\cos\theta_\mu dT_\mu$ (158 bins)				$d\sigma/dQ^2$ (15 bins)				$\sigma(E_\nu)$ / E_ν (18 bins)			
	χ^2_{diag}	χ^2_{tot}	χ^2_{sh}	N	χ^2_{diag}	χ^2_{tot}	χ^2_{sh}	N	χ^2_{diag}	χ^2_{tot}	χ^2_{sh}	N
GENIE 2.12.2	463.0	1146	1094	0.979	38.8	540.4	495.6	0.979	6.8	23.7	20.0	0.948
GENIE 3.00.06	224.4	1501	1965	1.137	17.5	25.5	36.5	1.189	13.5	25.2	34.5	1.123
NEUT 5.4.0	390.0	1743	1848	1.026	7.2	108.2	107.3	1.039	5.8	17.1	16.5	1.010
GiBBU 2019	602.0	1225	2050	1.285	58.4	117.6	211.5	1.351	43.3	61.0	123.3	1.169
NuWro 2019	218.7	647.9	882.7	1.163	19.9	55.2	72.0	1.224	13.9	9.9	12.0	1.141
NOvA Tune	25.6	281.3	283.1	1.004	2.3	4.7	4.8	0.959	1.8	27.4	25.7	0.944
MArun	124.6	669.8	821.8	1.105	7.6	29.1	32.0	1.115	7.3	33.6	31.5	1.021

$N \simeq 1.07 \simeq 1 + 0.62\delta$ required in the case of the normalization to the area), but this renormalization is still consistent with the uncertainty of the general normalization of data. In other words, the MArun model agrees with the measured cross sections $d^2\sigma/d\cos\theta dT_\mu$ within the experimental uncertainties, but a systematic distorsion of the predicted dependence of the cross section on the muon energy is observed for all models except for the NOvA Tune model and partially the GiBBU 2019 model. The degree of this distortion increases with $\cos\theta_\mu$.

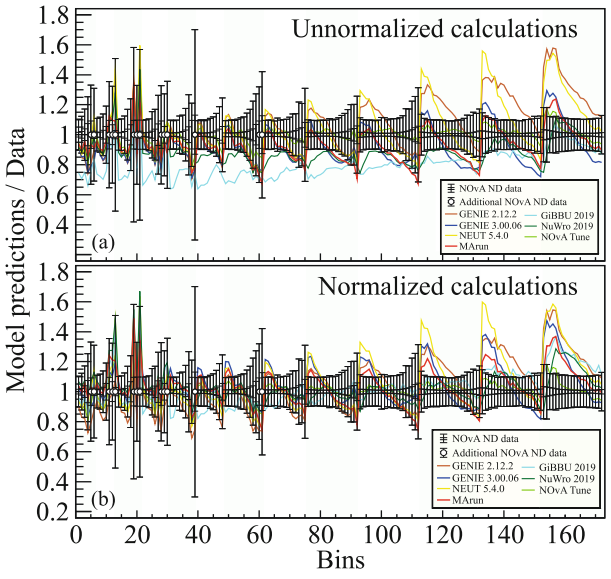

Fig. 6. (Color online) Ratios of the calculated double differential cross section $d^2\sigma/d\cos\theta_\mu dT_\mu$ averaged over the ν_μ spectrum to that measured in the NOvA near detector with the statistical and total (statistical plus systematic) errors versus the experimental bin number; the bins are enumerated from left to right and from top to bottom according to the first 13 panels of Fig. 1, and the vertical bars mark the $\cos\theta_\mu$ intervals indicated in these panels. The solid lines connected discrete values of the ratios for each of the seven models are plotted for the best visualization. Panels (a) and (b) correspond to unnormalized cross sections and cross sections normalized according to the procedure described in the main text, respectively.

Figure 7 shows the ratios of the calculated unrenormalized spectrum averaged (a) differential cross section $d\sigma/dQ^2$ and (b) slope of the total cross section $\sigma(E_\nu)/E_\nu$ for the same models in the linear binning representation to the corresponding experimental data presented in Fig. 2. The normalization coefficients and all three χ^2 characteristics are summarized in Table 2. As seen, model predictions and the normalization coefficients required for the best description of data for $d\sigma/dQ^2$ and $\sigma(E_\nu)/E_\nu$ also have a large spread from 0.96 (NOvA Tune) to 1.35 (GiBBU 2019), i.e., ~3.5δ, for $d\sigma/dQ^2$ and from 0.94 (NOvA Tune) to 1.17 (GiBBU 2019), i.e., ~2δ, for $\sigma(E_\nu)/E_\nu$. It is noteworthy that the tuning of the parameters of the NOvA Tune model to the double differential cross section data does not cancel the necessity of an additional, relatively small, renormalization for the description of data on $d\sigma/dQ^2$ and $\sigma(E_\nu)/E_\nu$.

The MArun model is also quite competitive in this application although deviations from the observed dependences of the cross sections on Q^2 and E_ν are seen for all considered models except for the NOvA Tune model. For the MArun model, discrepancies with the data are in most cases within the measurement errors. We note that the removal of only one last bin, to which deep inelastic scattering makes the decisive contribution and which weakly correlates with the remaining data (see Fig. 4) from the processing of the data in Fig. 7a noticeably improves the description of the dependence of $d\sigma/dQ^2$ on Q^2 so that the parameter χ^2_{sh}/n (where n is the number of bins) decreases from 2.1 to 1.6. Data on the slope of the total cross section $\sigma(E_\nu)/E_\nu$ demonstrate a similar but smaller effect: the removal of the last two (three) bins, where the contribution from cross sections for quasielastic scattering

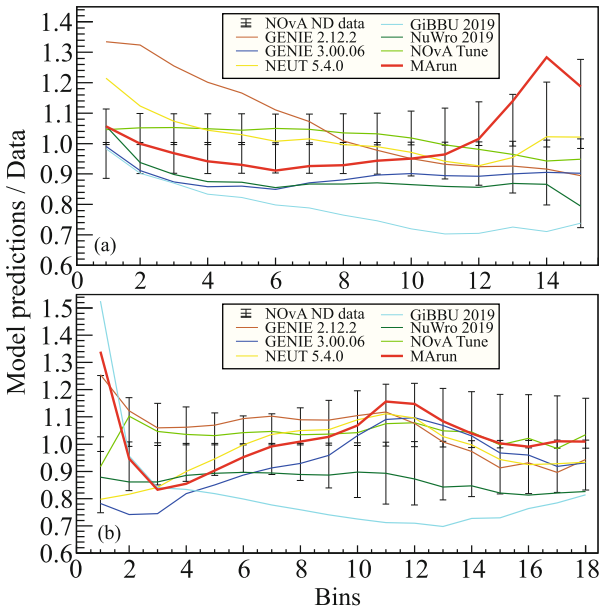

Fig. 7. (Color online) Ratios of the calculated unnormalized quantities (a) $d\sigma/dQ^2$ and (b) $\sigma(E_\nu)/E_\nu$ to measured ones with the statistical and total errors versus the experimental bin number; the bins are enumerated from left to right according to Figs. 2a and 2b, respectively. The solid lines connected certain ratios for each of the seven models are plotted for the best visualization.

weakly correlates and small ($\lesssim$10%), from the data in Fig. 7b reduces χ^2_{sh}/n from 1.75 to 1.56 (1.59). These examples indicate that the MArun model adequately describe the contributions from the cross sections for quasielastic and quasielastic-like scattering to the differential and total cross sections.

CONCLUSIONS

It has been shown that the model of running axial mass (MArun), which was developed to describe quasielastic and quasielastic-like scattering of neutrinos on nuclei, being used in the GENIE neutrino generator, which allows one to take into account inelastic channels and the interaction of secondary hadrons with nuclei, agrees well (without additional modifications and tuning) with recent NOvA near detector data. The MArun model in application to the calculation of inclusive cross sections for the scattering of neutrinos on nuclei is competitive with other models involved in the GENIE, NEUT, GiBBU, and NuWro generators and can be used along with them to analyze neutrino oscillation data obtained in the NOvA far detector. An additional fine tuning of the model to NOvA near detector data and/or the inclusion of these and other modern data in the extended global fit will make it possible to improve its predictive capabilities.

We note that, since meson exchange currents are taken into account in the MArun model empirically through the energy dependence of the parameter $M_A^{\rm run}$ rather than explicitly, it would be of interest to test the MArun model on data for semi-inclusive cross sections in the kinematic region sensitive to the contribution of exchange currents and, in particular, of $2p2h$ processes. This would allow one to determine more accurately the area of applicability of the model.

ACKNOWLEDGMENTS

We are grateful to Leonidas Aliaga, Linda Cremonesi, and Jonathan Paley for discussions of analysis of the details of the NOvA data and theoretical calculations and to Konstantin Kuzmin and Alexander Olshevskiy for useful comments.

FUNDING

This work was supported by the Ministry of Science and Higher Education of the Russian Federation (project no. 075-15-2024-541, National Program "Nauka" for funding of large scientific projects).

CONFLICT OF INTEREST

The authors of this work declare that they have no conflicts of interest.

OPEN ACCESS

REFERENCES

1. M. A. Acero, P. Adamson, L. Aliaga, et al. (NOvA Collab.), Phys. Rev. D **107**, 052011 (2023).
2. A. Cudd (on behalf of the T2K Collab.), Phys. Sci. Forum **8**, 14 (2023).
3. V. Hewes, B. Abi, R. Acciarri, et al. (DUNE Collab.), Instruments **5** (4), 31 (2021).
4. K. Abe, H. Aihara, C. Andreopoulos, et al. (Hyper-Kamiokande Proto-Collab.), Prog. Theor. Exp. Phys. **2015**, 053C02 (2015).

5. K. Abe, R. Abe, S. H. Ahn, et al. (Hyper-Kamiokande Proto-Collab.), Prog. Theor. Exp. Phys. **2018**, 063C01 (2018).
6. A. V. Akindinov, E. G. Anassontzis, G. Anton, et al. (P2O Proto-Collab.), Eur. Phys. J. C **79**, 758 (2019).
7. K. S. Kuzmin, V. A. Naumov, and O. N. Petrova, Phys. Part. Nucl. **48**, 995 (2017).
8. I. D. Kakorin, K. S. Kuzmin, and V. A. Naumov, Phys. Part. Nucl. Lett. **17**, 265 (2020).
9. I. D. Kakorin, K. S. Kuzmin, and V. A. Naumov, Eur. Phys. J. C **81**, 1142 (2021).
10. L. Alvarez-Ruso, C. Andreopoulos, A. Ashkenazi, et al. (GENIE Collab.), Eur. Phys. J. ST **230**, 4449 (2021).
11. R. A. Smith and E. J. Moniz, Nucl. Phys. B **43**, 605 (1972); Nucl. Phys. B **101**, 547(E) (1975).
12. K. S. Kuzmin, V. V. Lyubushkin, and V. A. Naumov, Eur. Phys. J. C **54**, 517 (2008).
13. V. Lyubushkin, B. Popov, J. Kim, et al. (NOMAD Collab.), Eur. Phys. J. C **63**, 355 (2009).
14. A. A. Aguilar-Arevalo, C. E. Anderson, A. O. Bazarko, et al. (MiniBooNE Collab.), Phys. Rev. D **81**, 092005 (2010).
15. A. A. Aguilar-Arevalo, B. C. Brown, L. Bugel, et al. (MiniBooNE Collab.), Phys. Rev. D **88**, 032001 (2013).
16. K. Abe, J. Amey, C. Andreopoulos, et al. (T2K Collab.), Phys. Rev. D **98**, 032003 (2018).
17. K. Abe, J. Amey, C. Andreopoulos, et al. (T2K Collab.), Phys. Rev. D **97**, 012001 (2018).
18. D. Ruterbories, K. Hurtado, J. Osta, et al. (MINERvA Collab.), Phys. Rev. D **99**, 012004 (2019).
19. C. E. Patrick, L. Aliaga, A. Bashyal, et al. (MINERvA Collab.), Phys. Rev. D **97**, 052002 (2018).
20. A. A. Aguilar-Arevalo, B. C. Brown, L. Bugel, et al. (MiniBooNE Collab.), Phys. Rev. Lett. **120**, 141802 (2018).
21. D. Rein and L. M. Sehgal, Ann. Phys. (N.Y.) **133**, 79 (1981).
22. K. S. Kuzmin, V. V. Lyubushkin, and V. A. Naumov, Mod. Phys. Lett. A **19**, 2815 (2004).
23. C. Berger and L. M. Sehgal, Phys. Rev. D **76**, 113004 (2007).
24. I. D. Kakorin and K. S. Kuzmin, Phys. Rev. D **104**, 093001 (2021).
25. K. S. Kuzmin, V. V. Lyubushkin, and V. A. Naumov, Acta Phys. Polon. B **37**, 2337 (2006).
26. R. L. Workman, V. D. Burkert, V. Crede, et al. (Particle Data Group), Prog. Theor. Exp. Phys. **2022**, 083C01 (2022).
27. P. Rodrigues, C. Wilkinson, and K. McFarland, Eur. Phys. J. C **76**, 474 (2016).
28. M. A. Acero, P. Adamson, G. Agam, et al. (NOvA Collab.), Eur. Phys. J. C **80**, 1119 (2020).
29. C. Andreopoulos, A. Bell, D. Bhattacharya, et al. (GENIE Collab.), Nucl. Instrum. Methods Phys. Res., Sect. A **614**, 87 (2010).
30. C. Andreopoulos, C. Barry, S. Dytman, H. Gallagher, T. Golan, R. Hatcher, G. Perdue, and J. Yarba, arXiv: 1510.05494 hep-ph (2015).
31. J. Tena-Vidal, C. Andreopoulos, A. Ashkenazi, et al. (GENIE Collab.), Phys. Rev. D **104**, 072009 (2021).
32. J. Tena-Vidal, C. Andreopoulos, C. Barry, et al. (GENIE Collab.), Phys. Rev. D **105**, 012009 (2022).
33. Y. Hayato, Nucl. Phys. B Proc. Suppl. **112**, 171 (2002).
34. G. Mitsuka, AIP Conf. Proc. **981**, 262 (2008).
35. Y. Hayato, Acta Phys. Polon. B **40**, 2477 (2009).
36. T. Golan, J. T. Sobczyk, and J. Zmuda, Nucl. Phys. B Proc. Suppl. **229–232**, 499 (2012).
37. T. Golan, C. Juszczak, and J. T. Sobczyk, Phys. Rev. C **86**, 015505 (2012).
38. O. Buss, T. Gaitanos, K. Gallmeister, H. van Hees, M. Kaskulov, O. Lalakulich, A. Larionov, T. Leitner, J. Weil, and U. Mosel, Phys. Rep. **512**, 1 (2012).
39. K. Gallmeister, U. Mosel, and J. Weil, Phys. Rev. C **94**, 035502 (2016).
40. U. Mosel, J. Phys. G **46**, 113001 (2019).
41. J. Campbell, M. M. Diefenthaler, T. J. Hobbs, et al. (Initiative Group on Part. Fields), in *Proceedings of the 2021 US Community Study on the Future of Particle Physics (Snowmass 2021),* Ed. by J. N. Butler, R. Sekhar Chivukula, and M. E. Peskin (APS Div. Part. Fields, 2022); arXiv: 2203.11110 [hep-ph].
42. NOvA Collab., Data Releases, 2024. https://novaexperiment.fnal.gov/data-releases/.

Translated by R. Tyapaev